

PAPER • OPEN ACCESS

## PDMS-polyimide transcutaneous blood gas collector with self-folding out-of-plane heater elements

To cite this article: Ragnar Seton *et al* 2023 *J. Micromech. Microeng.* **33** 065006

View the [article online](#) for updates and enhancements.

### You may also like

- [Chest tcpO<sub>2</sub> changes during constant-load treadmill walking tests in patients with claudication](#)  
N Ouedraogo, M Feuilloy, G Mahe et al.
- [Using a high-frequency carrier does not improve comfort of transcutaneous spinal cord stimulation](#)  
Ashley N Dalrymple, Charli Ann Hooper, Minna G Kuriakose et al.
- [Epidural and transcutaneous spinal cord stimulation facilitates descending inputs to upper-limb motoneurons in monkeys](#)  
Thomas Guiho, Stuart N Baker and Andrew Jackson

# PDMS-polyimide transcutaneous blood gas collector with self-folding out-of-plane heater elements

Ragnar Seton<sup>1,\*</sup> , Zahra Khaji<sup>2</sup>  and Anders Persson<sup>1</sup> 

<sup>1</sup> Division of Microsystems Technology, Department of Material Science and Engineering, Uppsala University, Uppsala SE-75121, Sweden

<sup>2</sup> Division of Biomedical Engineering, Department of Material Science and Engineering, Uppsala University, Uppsala SE-75121, Sweden

E-mail: [ragnar.seton@angstrom.uu.se](mailto:ragnar.seton@angstrom.uu.se)

Received 9 December 2022, revised 28 February 2023

Accepted for publication 4 April 2023

Published 26 April 2023



## Abstract

This paper introduces and evaluates a novel, highly scalable fabrication technique for folding flexible printed circuit board (PCB) features into polydimethylsiloxane (PDMS). The technique is then used to create fast and effective skin-heaters in a prototype gas collector for transcutaneous blood gas monitoring (TBM), a well-established technique to non-invasively measure the amount of CO<sub>2</sub> and O<sub>2</sub> in a patient's blood. Previous studies have shown that TBM can be made safer by heating the patient's skin with short pulses rather than continuously. Hence, the effects of incorporating a resistive heater with folded heating elements into a PDMS gas collector was investigated and compared to a heater with surface mounted heating elements. The results show that the fabrication technique provides consistent, controllable folding angles using only the surface and viscous forces of the flexible PCB and PDMS. With the investigated design- and material parameters a maximum folding angle of 30° was achieved, resulting in a 2000% increase in initial surface heating compared to an un-folded reference. For the intended application, this corresponds to reducing the time needed to heat the skin of a patient to less than half. The presented fabrication technique is, however, not limited to the application investigated in this paper, but rather offers the possibility to quickly and automatically fold complex structures and circuits into the bulk of the PDMS without introducing any time overhead as the number of features and folds grow.

Keywords: PDMS, flexible PCB, transcutaneous blood gas monitoring, self-folding

(Some figures may appear in colour only in the online journal)

## 1. Introduction

Transcutaneous blood gas monitoring (TBM) is a medical technique to non-invasively measure the amount of CO<sub>2</sub> and

O<sub>2</sub> in a patient's blood by analyzing the minute amounts of gas that continuously diffuse through the skin. Conventional TBM methods rely on equilibration of the partial pressures of the two gases in a small sealed volume with one side open to the skin, inside which miniaturized gas sensors are mounted [1]. TBM has found major use in neonatal care, to monitor the respiratory and circulatory status of preterm infants. In this application, the conventional solutions suffer from some limitations, primarily stemming from the need to heat the skin of the patient to 43 °C or more to make it permeable enough for reliable measurements. This makes the monitoring intermittent

\* Author to whom any correspondence should be addressed.



Original content from this work may be used under the terms of the [Creative Commons Attribution 4.0 licence](https://creativecommons.org/licenses/by/4.0/). Any further distribution of this work must maintain attribution to the author(s) and the title of the work, journal citation and DOI.

instead of continuous, since it has to be aborted after about an hour to avoid the formation of harmful burns [2, 3]. However, the heating also offers some advantages as it dilates the cutaneous capillaries and allows for increased arterial blood flow close to the skin. The arterialization of the cutaneous blood flow, and hence the blood gas levels, gives the caregiver more relevant information about the patient's health, since the monitoring otherwise, partly, reflects the metabolism in the local tissue below the probe [1]. Other problems include the size and stiffness of the probe, since equilibration requires it to be hermetically sealed from the atmosphere. The stiff enclosure requires it to be attached to a flat surface of the skin, and due to its size (20 mm) attachment becomes limited to the torso of a neonate. There, it has to compete for space with other medical technology, such as electrocardiogram (ECG) electrodes [4].

A previous study [5], presented a novel transcutaneous blood gas collector made from soft and flexible polydimethylsiloxane (PDMS), which enabled attachment to curved surfaces on the skin and hence made it easier to use for a caregiver. However, this first prototype did not contain a heater and hence did not enable monitoring of arterialized gas levels. Moreover, the lack of an electrical interface made it difficult to integrate with other forms of monitoring—such as pulse oximetry, ECG, and respiration—which is highly sought after in neonatal intensive care [4].

The present study explores the possibility to introduce electrical heaters in the PDMS design, by integrating it with a polyimide-copper (PI-Cu) flexible printed circuit board (PCB). The added electrical interface would, however, not be limited to just heaters. Conventional TBM systems have for some time been complemented with other types of sensors, like the aforementioned pulse oximeter and also temperature sensors, and the addition of an electrical interface to the PDMS design would provide the option to integrate such functionality in it as well.

PI-PDMS laminates is a common material combination in soft microsystems as they combine compatibility with rapid PCB manufacturing processes with bio-friendliness. They have previously been used for sensor integration in microfluidics [6], tactile surfaces in robotics [7], and wearable intrabody communication systems [8]. However, PI-PDMS systems usually only allow for the bonding of 2D surface structures. This can be a disadvantage in the present application due to the low thermal conductivity of both PDMS and PI which makes it problematic to transfer the heat created with, e.g. resistive Cu heaters on the PI substrate through the PDMS to the skin. Hence, it would be advantageous to be able to fold the heaters out of the PI plane, into the bulk of the PDMS, to position them closer to the skin interface. Interesting in this respect is the use of PI substrates in different self-assembly schemes like self-folding origami-like microsystems. Examples of folding mechanisms are selective laser heating [9], shape memory effects [10], and capillary forces [11]. Although all these methods are feasible, they may be too complex and costly for the large-scale production of gas collectors in a future commercial case, given that the gas collector will be a disposable item

and hence needs to be produced in large batches of more than 10 000 pieces per day.

To find a fabrication technique more suitable to such large-scale production, we investigate a much simpler folding mechanism—how the viscous and surface forces that are active during the casting and curing of PDMS can be used to fold PI features into the bulk of it. The underlying principle is to let PI micro-flaps, connected by Cu hinges to the surrounding PI, self-fold into the PDMS while it is cured. To investigate the usefulness of this technique, PI flaps with varying hinge dimensions, flap surface areas and aspect ratios were fabricated and cast into PDMS, and their final folding angle was measured using image analysis of their micrographs. In addition to these design parameters, the surface tension and viscosity of the uncured PDMS and the surface energy of the flaps were varied. The most promising folding design was then used to create a prototype of a transcutaneous blood gas collector with out-of-plane heater elements, and its ability to quickly and effectively heat the skin was evaluated by comparing it to a similar device with surface-mounted heaters.

## 2. Materials and methods

For the initial experiments evaluating the folding angle's dependence on the design parameters of the flaps and hinges, four sets of samples were designed using 2022 development snapshots of the open source software OpenSCAD. The samples were fabricated from a Cu (12  $\mu\text{m}$ ) PI (25  $\mu\text{m}$ ) substrate (DSflex-600, Doosan Electro-Materials, South Korea), each consisting of two contact pads (one shared) and a flap of varying length and width. The PI layer of the flap was fully released from its surrounding through laser ablation, leaving it connected to the rest of the substrate by two Cu traces, here referred to as hinges. The hinges were made by wet etching prior to the laser ablation, and had varying lengths and widths as well. The first sample set, top left in figure 1(a), had constant,  $800 \times 800 \mu\text{m}$  flap areas, hinge lengths of 100  $\mu\text{m}$ , and hinge widths varying from 100  $\mu\text{m}$  to 300  $\mu\text{m}$ . The second sample set (top right in the figure) had fixed flap areas of  $800 \times 400 \mu\text{m}$ , hinge widths of 100  $\mu\text{m}$ , and hinge lengths varying from 100  $\mu\text{m}$  to 500  $\mu\text{m}$ . In the third and fourth sample sets, the hinges were fixed at  $100 \times 100 \mu\text{m}$ , and the former varied the flap aspect ratio from 3:8 to 8:3 while the latter varied the flap area from  $300 \times 300 \mu\text{m}$  to  $800 \times 800 \mu\text{m}$  (bottom row in figure 1(a)). All ranges were divided into nine equidistant steps. Four replicates of each sample set made batches with a total of  $4 \times 9 \times 4$  samples, measuring just under  $23 \times 16 \text{ mm}$ . This area was chosen to ensure that the batches could be fitted in the field of view of the vision system (FH-2050 with FH-SC21R camera, OMRON, Japan) used for alignment in the laser ablation step of the fabrication process.

The Cu mask patterns, the red traces in figure 1, were created by applying a positive mask to the Cu side of the substrate using a standard toner transfer method [12]. This process entailed printing the mask onto transparency film using a laser printer (MP C5504ex, Ricoh, Japan) at 1200

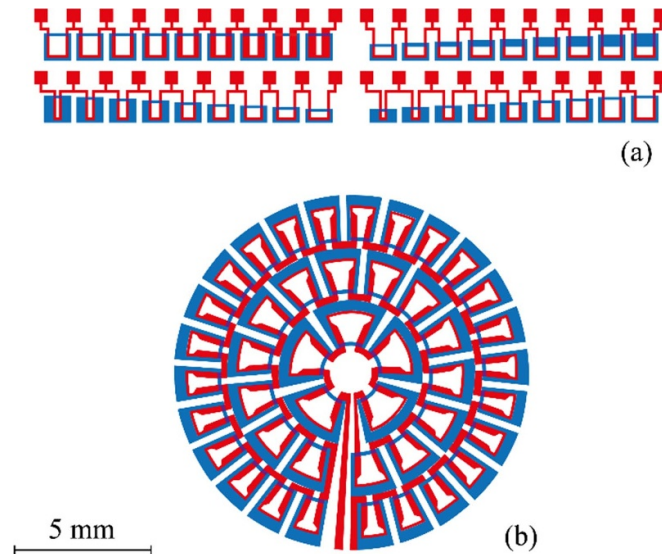


**Figure 1.** Positive Cu etching mask (red) and PI ablation areas (blue) for the folding experiment samples (a) and prototype blood gas collector (b).

dots per inch (DPI) resolution, and then transferring it onto the substrate with a consumer grade laminator (Exibel L402-A, Clas Ohlson AB, Sweden) at just over 130 °C. The lamination process included taping the substrate onto the printed mask using Scotch tape (3M, USA) and then feeding it through the laminator three times. The PI and transparency film were then separated while cooling down, before reaching the ambient temperature of 22 °C. Separating them immediately as they exited the laminator was found to cause smearing of the mask, while waiting until they cooled down fully risked causing cracks, especially in high aspect ratio features. It is worth noting that the resolution and consistency of the printed mask depended heavily on the software and file formats used to produce the digital, vectorized mask. The workflow that reliably produced prints where the resolution was limited by the printer DPI setting was: (i) exporting the mask as a scalable vector graphics (SVG) from OpenSCAD, (ii) adjusting the stroke-width of the SVG using search and replace in any text editor, e.g. sed, (iii) converting the SVG (also converting any text to paths) to a PDF using Inkscape v1.1.2, (iv) ensuring that scaling and image smoothing was turned off when printing. While this process is hardware and printer driver dependent, image smoothing is a feature offered (and often turned on by default) by most printers. With a workflow in place that produced high quality prints, the toner transfer method offered rapid prototyping of masks with features down to 100  $\mu\text{m}$ .

Following the mask transfer, the traces were etched in an agitated, 200 g sodium persulfate per liter water bath, kept at a constant temperature of 35 °C. At this solution and temperature, the etch-rate averaged close to 1  $\mu\text{m min}^{-1}$ . After etching, the PI substrate was cleaned in four steps using deionized water, isopropyl alcohol (IPA), acetone, and finally IPA again. The PI was then ablated with the blue pattern in figure 1, using a laser marker (AIO G+532 nm 5 W, Östling Märksystem AB, Sweden). With the precision provided by the previous fabrication steps, explicit alignment markers were found to be

superfluous when using the vision system. Instead, the corners of the Cu traces were used to align the CAD file with the position of the PI substrate in the laser chamber. The precision of this alignment method was high enough to instead make the drift of the laser the primary source of errors in the ablation.

After ablation, the batches were ready for PDMS casting. In the initial experiments, only Sylgard 184 (S184) (Dow Corning, USA) PDMS was used. The PI was first taped to the bottom of a petri dish, again using Scotch tape, with the Cu side facing downward. The PDMS was then mixed in a centrifugal mixer (ARE-250, Thinky Corp., Japan) and poured onto the PI, figure 2(a), and immediately placed in a vacuum desiccator (Nalgene 5311-0250, Thermo Fisher Scientific, USA), pumping (Laboport N 840.1.2 FT.18, KNF Neuberger GmbH, Germany) it to a low, >90 mbar, vacuum to extract all the trapped air. The PDMS casts were then left to cure at room temperature for 72 h.

When the PDMS had cured, the folding angle of the flaps was determined manually, in two steps. Firstly, each individual flap was photographed (Infinity X-21, Deltapix, Denmark) in a backlit microscope (AX70, Olympus Corp., Japan), retaining metadata that included two lateral pixel dimensions-to- $\mu\text{m}$  conversion constants. The images were then imported into a purpose-built MATLAB application<sup>3</sup> where the dimensions of the ablated area and folded flap were measured by manually overlaid rectangles. The former was used to ensure that the substrate was mounted flat against the petri dish and as a per-flap ablation precision measure. For the flaps, the adjacent length,  $a$ , i.e. the 1D projection of the top surface of the PI flap, was used to determine the folding angle  $\alpha = \cos^{-1}(a/l)$ , where  $l$  is the length of the surface, as shown in figure 2(a). To verify the angles calculated with this method, parallel measurements were performed with an optical profilometer

<sup>3</sup> Full implementation available in [15].

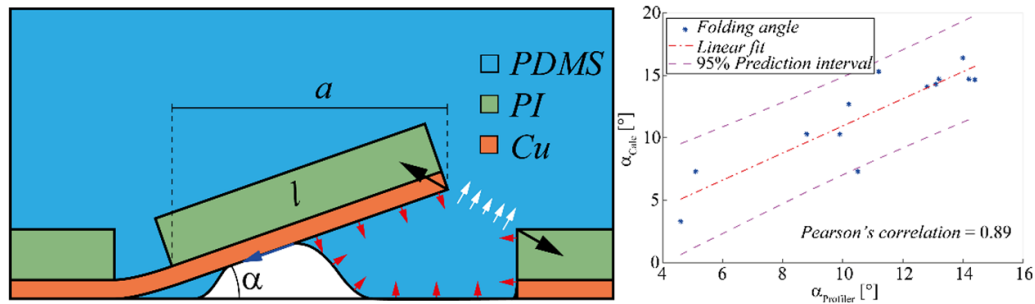


**Figure 2.** (a) Schematic overview of the folding process. The surface forces are visualized by red and blue arrows for the Cu-PI substrate and PDMS, respectively, viscous forces by white arrows, and the resulting folding force by black arrows. The length  $a$  (the 1D-projection of  $l$ ) was measured to determine the folding angle  $\alpha$ . (b) Correlation between surface profilometer angle measurements of heater flaps and the corresponding angles calculated using the method illustrated in (a).

(NexView NX2, Zygo Corp., USA). The profilometer was, however, unable to measure folding angles greater than  $\sim 20^\circ$  due to light scattering in the PDMS and poor vertical reflection. The subset of flaps that were measured showed a good correlation between the methods, figure 2(b), with a Pearson's correlation coefficient of 0.89. Hence, the microscopy method was deemed adequate for subsequent measurements.

### 2.1. Viscosity, surface tension and surface treatment experiments

The second set of experiments varied the surface properties of the PI, and surface tension and viscosity of the uncured PDMS. For the former, three different surface treatments were applied to individual sample batches, (i) a 60 s low intensity air plasma treatment (BD-50E Heavy Duty Generator, Electro-Technic Products, USA), (ii) a high intensity plasma treatment of the same length (with about twice the power of (i)), and (iii) a hydrophobic primer, hexamethyldisilazane (HMDS-Primer, Micro resist technology GmbH, Germany) applied through vapor deposition, using a Star 2000 vapor prime vacuum oven (Imtec, USA). As the surface activation of treatments (i) and (ii) decayed quickly, the PDMS was dispensed onto the samples within 30–40 s after the treatments were finished.

The surface tension and viscosity of the catalyzed but uncured PDMS was varied by using three different brands: True Skin 10 (CHT, USA), S184, and Elastosil Vario 15 (Wacker Chemie AG, Germany), and by varying the dispensing temperature of it. In the latter experiment only S184 was used, and its temperatures was set to  $-20^\circ\text{C}$ ,  $6^\circ\text{C}$ ,  $23^\circ\text{C}$ , and  $38^\circ\text{C}$ , all measured using a K-type thermocouple connected to a TM-947SD (Lutron, Taiwan) thermometer as the PDMS was dispensed onto the PI. Given the general low thermal conductivity of PDMS, the time from mixing to casting differed with temperature—the first two mixes were cooled in a freezer and refrigerator, respectively, for 18 h. The  $23^\circ\text{C}$  mix was cast directly after mixing, and the  $38^\circ\text{C}$  mix was heated in an oven for 30 min. While the viscosities of the different brands were given by their respective data sheets, the temperature dependence of the viscosity was modeled using a Weibull function,

as described in [13]. Similarly, the temperature dependence of the surface tension was modeled with the method described in [14].

### 2.2. Thermographic evaluation of prototype

Having found a combination of design-, viscous and surface parameters that provided consistent folding, a prototype of the transcutaneous gas collector with an integrated heater was designed by using the hinges as electrical connectors to a resistive heating element at the upper end of each flap, figure 1(b). These heater flaps formed three concentric circles on a round sample with a total, pre-folding diameter of 12.8 mm. All the flaps were electrically connected in series. The lengths and widths of the hinges were  $200 \times 200 \mu\text{m}$ , and the width of the heater element traces were 100  $\mu\text{m}$ . The total resistance of the heater circuit was  $\sim 2 \Omega$ .

Two such samples were fabricated using the method described above. However, the flaps of one of them were never released but remained bound to the PI surface to be used as a reference. After ablation, 0.25 mm enameled connection wires (1230976, Rowan Cable Products Ltd, UK) were soldered to the samples before casting each in a 1 mm thick layer of  $-20^\circ\text{C}$  S184. After curing, the samples were connected to a variable power supply (QL355TP, Aim-TTi, UK), and placed next to each other, in view of a 3rd Generation FLIR ONE Pro thermal imaging camera. The heaters, that had been cooled to room temperature before each measurement, were fed with power between 100 and 400 mW, while recording the resulting surface temperature of the samples for up to 90 s in an 8.8 fps video. Moreover, reference images were taken before and after each video, the latter while the power was still on. This was necessary as the video recordings did not contain the raw thermal data, only grayscale frames. Thermal data was instead calculated from the reference images, and used in the analysis to transform grayscale intensities from the videos to absolute temperatures. Hence, the analysis steps for each video were: (i) reading the second reference picture, (ii) reading the grayscale intensities from the video, (iii) generating a pixel-intensity-to-temperature (spline interpolation based) lookup table from

reference image and last frame of the video, (iv) identifying the regions of interest (ROIs) in each frame (figure 7(b)), and, (v) using the lookup table to determine the average temperatures within the ROIs in each frame. To mitigate any compression artefacts, the temperatures of the heaters were averaged over the disk-shaped ROIs with radii of about three quarters of the heaters. This analysis was automated in MATLAB, with the full implementation available together with the raw data in [15].

### 3. Results

The overall results showed that the process yielded consistent folding angles of up to about  $30^\circ$ . Figure 3(a) shows a micrograph of one of the blood gas collectors where both the folding and the general quality of the fabrication process can be assessed. For further details of the folding figure 3(b) shows an example of the surface profile of the copper of a single heater flap measured with the optical profilometer.

The initial experiments showed that the design parameters of the flaps and hinges had a limited effect on the folding angle within the tested ranges, figure 4, where the groups are defined as described in section 2. Particularly the area and aspect ratio of the flaps had no significant influence on the folding angle, figures 4(c) and (d). The experiments did, however, provide a lower bound to the mechanical strength of the hinges. The weak inverse relationship between hinge length and folding angle was primarily caused by the flaps being pushed parallelly up from the surrounding PI, folding the hinges in two places rather than one, which caused widely inconsistent folding angles as indicated by the whiskers in figure 4(b). Wider hinges provided a much more consistent folding angle, figure 4(a). The trend of increasing angles with increasing hinge widths also indicated that the implicitly investigated range of hinge strengths were in the lower end of what the folding technique is suitable for.

To highlight the influence of viscosity and surface tension on the folding mechanism, figure 5 only shows the folding angles of flaps with constant hinge width, which was the design parameter set with the smallest intraset median folding angle variation. Even though the intragroup folding angles varied, the left part of the figure indicates that the folding angle appeared to increase with lower temperature, i.e. higher surface tension and viscosity, as both increase with falling temperatures [13, 14]. This is further supported by the right part of the figure where the PDMS brands are ordered by decreasing viscosity from left to right. In addition to folding angle, the folding consistency also increase with the surface tension and viscosity.

Finally, figure 6 shows that the hydrophilic surface treatment of the PI significantly reduced the folding of the flaps, and that the hydrophobic primer fully eliminated the effect. The few outliers seen with the primer in figure 6 were primarily explained by the slight folding that would occur during PI ablation and mounting the substrate inside the petri dish. Hence, the fabrication technique offered methods for both consistently folding features of arbitrary shapes, as well as the

possibility to reliably, and potentially selectively, stop features from folding.

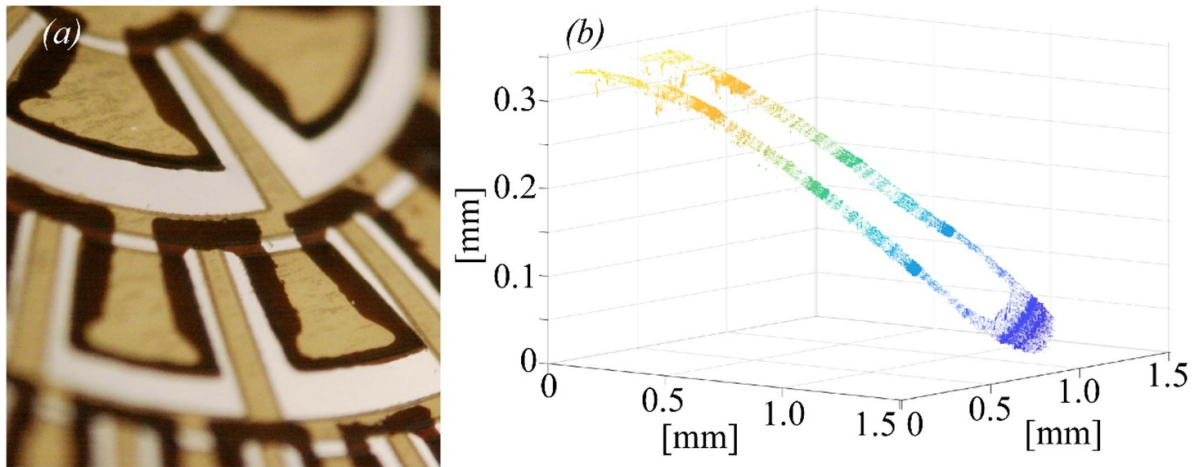
#### 3.1. Blood gas collector prototype

Figure 7(a) shows a photograph of the heater evaluation setup, and (b) a representative video frame of the two blood gas collector prototypes during heating. As can be seen, the distribution of the surface temperature was both smooth and symmetric indicating well-functioning resistive heaters. The prototype with folded heaters showed considerable improvements over the flat reference, both with respect to the maximum surface temperature and temperature increase. In figure 7(c) the calculated surface temperature over time for the two samples is shown together with fitted power models. It should be noted that most of the variations in the results could be attributed to noise in the thermal camera, but that the power models correspond well to the expected thermal output. The most significant difference between the two heaters was the initial thermal response, where, e.g. the flat reference heater took 5.5 s longer to even measurably increase its surface temperature at the lowest investigated power.

### 4. Discussion

The folding mechanism observed in this study was primarily attributed to the interaction between three fluidic properties affecting the flaps while the PDMS was deposited and cured: (i) the surface energy of the PI, (ii) the surface tension of the PDMS, and (iii) the viscosity of the uncured PDMS. As the PDMS was deposited onto the PI, the net surface force in the three-phase boundary acted to minimize the liquid–gas interface, effectively pulling the PDMS along the surface of the flap, visualized by the blue arrow in figure 2(a). While the PDMS was being distributed along the PI, the surface tension in the liquid gas-interface acted to minimize its surface to volume ratio, shown as red arrows in the figure. When the front of the PDMS reached the bottom side of the flap, this force started to form a droplet with increasing volume that lifted the flap upwards from the substrate. Both of these processes depended on the viscosity of the PDMS, as it simultaneously restricted the progression speed along the PI and the fluid flow that caused the inflation of the droplet. It is this relation, between the progression speed and volume inflation, that results in the net folding forces applied between the flap and the PI, shown as black arrows in figure 2(a). While it would be possible to optimize this process for the general case of applying a net force in an arbitrary direction on the solid under which the PDMS is pulled, this would entail exploring a much larger parameter space spanning wider surface tensions, viscosities, and PI surface energies, which was beyond the scope of this exploratory investigation.

However, some general reflections regarding such optimization and the balancing of the relevant forces can still be made based on the experiments performed here. First, a very high surface energy would pull the PDMS all the way along the bottom side of the flap before the droplet has time to inflate, hence



**Figure 3.** (a) Micrograph of folded flaps on the transcutaneous blood gas collector prototype. The width of the flap in the lower right corner was 1.3 mm. (b) Cu surface profile of a folded flap measured with the optical profilometer.

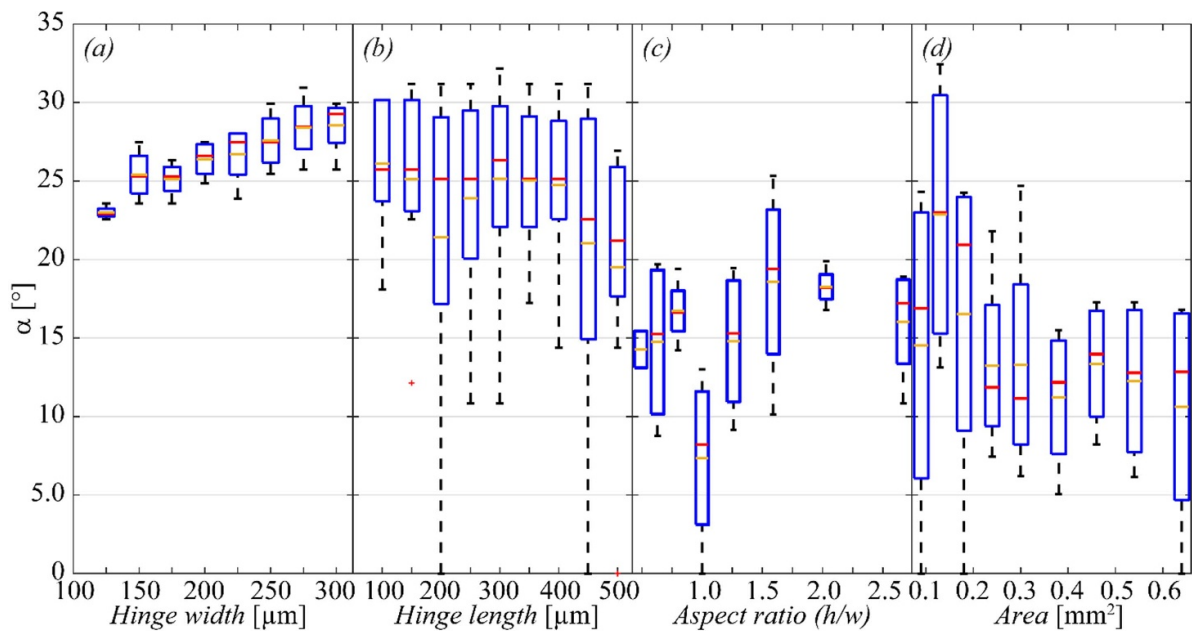


**Figure 4.** Folding angle as function of the different design parameters. The red and yellow lines indicate median and mean values, respectively. The blue boxes cover the interquartile ranges (IQRs), and whiskers have a maximum length of 1.5 IQR, any value beyond 1.5 IQR are considered outliers and marked by a red +.

reducing the folding angle. In figure 6, the use of a hydrophobic primer illustrates this effect, where an increased surface energy reduced, and even eliminated, the folding entirely. This effect could also partly explain the results in figure 4(b), as an inflating droplet covering the whole bottom side of the flap would lift, rather than fold it. A reduced surface energy could, on the other hand, hinder the PDMS from properly wetting along the bottom of the flap, as indicated by the results of plasma treatment in figure 6.

Regarding surface tension, a higher tension would instigate quicker inflation, and hence more folding, up to a point where the surface tension is too high to allow the PDMS to wet to the backside of the flap. A very low surface tension

would, on the other hand, allow the PDMS to form a thin film on the backside of the flap resulting in minimal folding. These assumptions were supported by the results in figure 8(a) where the folding angle increased linearly with surface tension as the PDMS was cooled. The linear dependence indicated that the limiting level was far higher than the tensions explored in this study, and, hence, that the proposed method could produce folding angles much larger than the observed  $\sim 30^\circ$ . It should be noted that the surface tension was modeled based on the measured temperature and molecular weight of S184 obtained from [16], using the method described in [14]. This method was based on experimentally obtained values for surface tensions of unspecified PDMSs with three different molecular

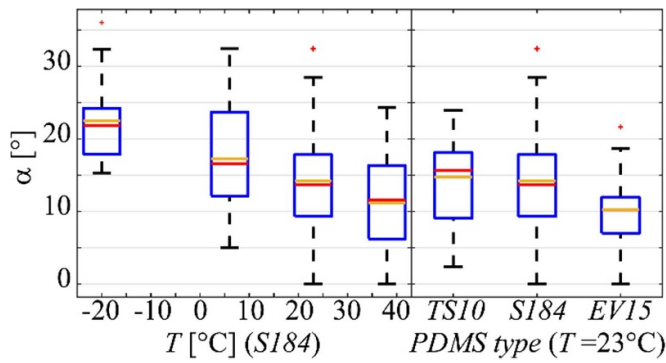


**Figure 5.** Folding angle as a function of temperature (left) and viscosity (right) of the uncured but activated PDMS used in casting. Each box represents the group of patches with varying flap size but constant hinge length and width. In the PDMS type boxplot TS10 and EV15 refers to True Skin 10 and Elastosil Vario 15, respectively.

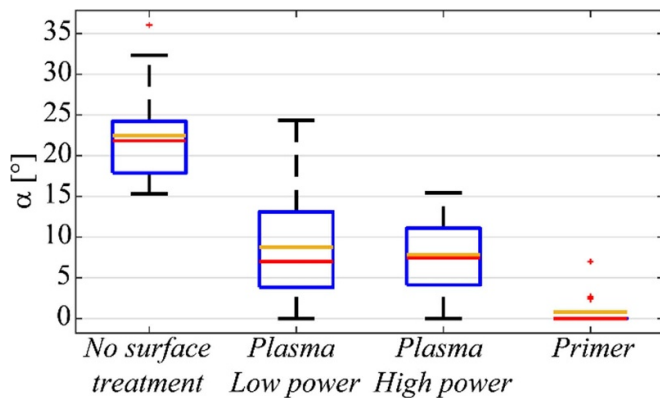


**Figure 6.** Folding angle as a function of surface treatments. As in figure 5 each box represents a patch group with varying flap sizes, however here all boxes are based on S184 cooled to  $-20\text{ }^{\circ}\text{C}$ .

weights,  $M_n$ :  $770\text{ g mol}^{-1}$ ,  $2600\text{ g mol}^{-1}$ , and  $32\,000\text{ g mol}^{-1}$ . The models created in [14] for the different  $M_n$  are all, for the temperature spans used here, linear to a root mean square relative error of less than 0.13%, and as the difference in slope per  $\text{g mol}^{-1}$  between the 2600 and 32 000 models is less than  $2 \times 10^{-7}$ , the error of a relative change approximation of the viscosity of the  $6243\text{ g mol}^{-1}$  S184, based on the 2600 model, was expected to be negligible.

Finally, regarding viscosity, too viscose PDMS could slow both the wetting and inflation of the droplet to a point where it starts to cure and the folding is quenched before the flap reaches its maximum angle. In figure 5 (left), the surface tension and viscosity were increased simultaneously by reducing the temperature of the PDMS, but figure 8(b) still shows that the increase in surface tension dominated and the folding angle increased even though the PDMS became more viscose. However, it would likely be more beneficial to find a method of increasing the surface tension of the PDMS without increasing, but ideally reducing, its viscosity. One example of the viscosity's limiting effect could be found in the experiments with

the most viscose PDMS, where the size of the frame around the flap was found to influence the folding angle by increasing it with larger frames, as seen in figure 9. This was likely due to the relationship between flow resistance,  $R$ , and both the viscosity of the fluid,  $\mu$ , and the effective width of the orifice through which it was flowing,  $w$ , which according to Hagen Poiseuille's equation scales as  $R \sim \mu w^{-4}$ . Hence, if the viscosity is too high, the flow that inflates the droplet can be limited, but this effect can easily be countered by increasing the orifice through which the flow runs. This effect could be an additional explanation to the results in figure 4(b) where the PDMS would rather wet onto the bottom side of the flap from the wider orifice at the hinges at its top, figure 1(a), hence creating a lifting rather than a folding force. This observation was utilized in the design of the blood gas collector prototype, where the flaps were given wider orifices at their tops than at their hinges, figure 1(b). Still, the effect of the hinge width, or rather strength, on the folding could have been investigated in more detail, e.g. by using substrates with thicker Cu cladding, particularly since figure 4(a) indicated that stronger hinges offered a higher folding angle.

Based on these general discussions about the folding mechanism itself, some particular reflections about the usefulness of the presented fabrication technique to the intended application for TBM could be made. Figure 10 shows the initial thermal response at different powers, which increased with a factor of up to 20 with folded heaters. After 15 s, the difference in temperature between the folded and flat heaters was still between 20% and 40%, showing that the effect was more than momentary. Looking closer at the shape of the dotted curves in the bottom row of figure 10, they indicate that the improvement in response can be expected to hold over wide range of power levels as the initial peaks stay at, close to, a constant multiple of that of the reference heater, for all investigated levels.

By differentiating the power fits from figure 7(c) with respect to time, the temperature change of the heaters could be calculated, figure 11 (top row). In the bottom row of the figure the absolute difference between the two indicates when the flat heater overtook the folded one. In all cases, this happened when both heaters were reaching a near constant heating rate, as indicated by the difference in speed following these points never reaching above  $0.05\text{ }^{\circ}\text{C s}^{-1}$ , meaning that the folded heaters were both much faster in delivering heat and in reaching a steady surface temperature.

In summation, the results from the thermal evaluation clearly show that the reduced distance from the heating elements to the surface of the gas collector significantly increased heat transfer. Based on the power models from figure 7(c) the maximum temperature increase rose by at least  $4\text{ }^{\circ}\text{C s}^{-1}$  across all power levels, as seen in figure 12(a). With the gas collector mounted on a neonate's skin, with an expected temperature of around  $33\text{ }^{\circ}\text{C}$ , and a target temperature of  $43\text{ }^{\circ}\text{C}$ , this means that the folded heater would only need about 50% of the time and 90% of the power to deliver the required heat compared to its flat counterpart. It should also be noted that the flat heater had a higher temperature on its backside than at

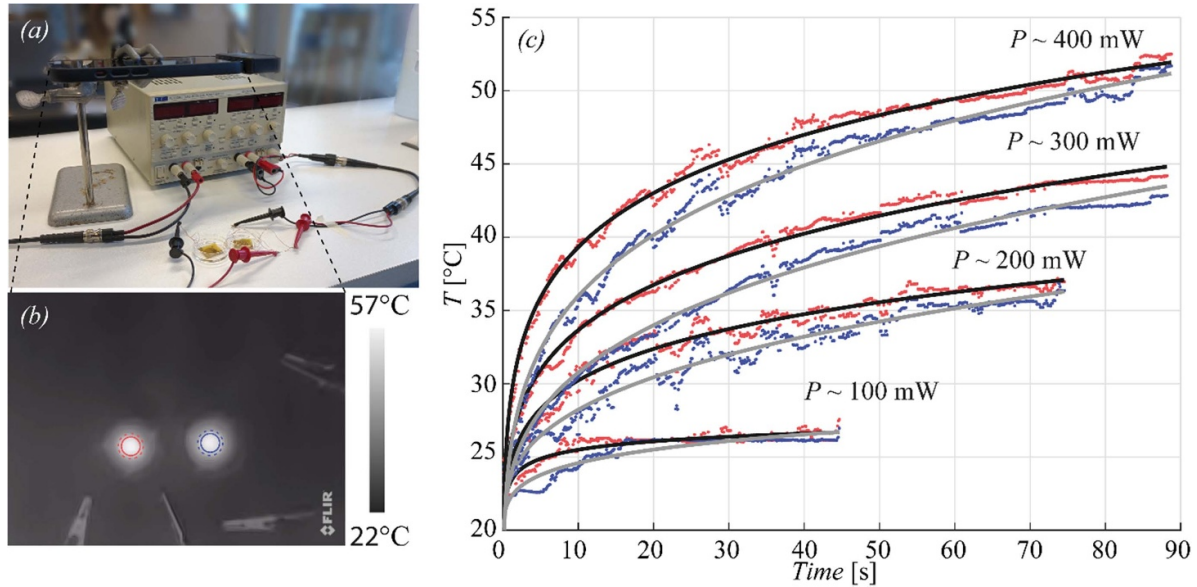


**Figure 7.** (a) The test setup showing, from top to bottom, the thermal camera connected to an iPhone 13, double output variable power supply, and the heater samples. (b) A cropped thermal video frame with the ROIs indicated by solid circles and outline of the heaters by dotted ones. (c) Measured temperatures of the folded prototype heater (red) and flat reference heater (blue) over time, for four different power inputs. The solid lines represent power model fits.

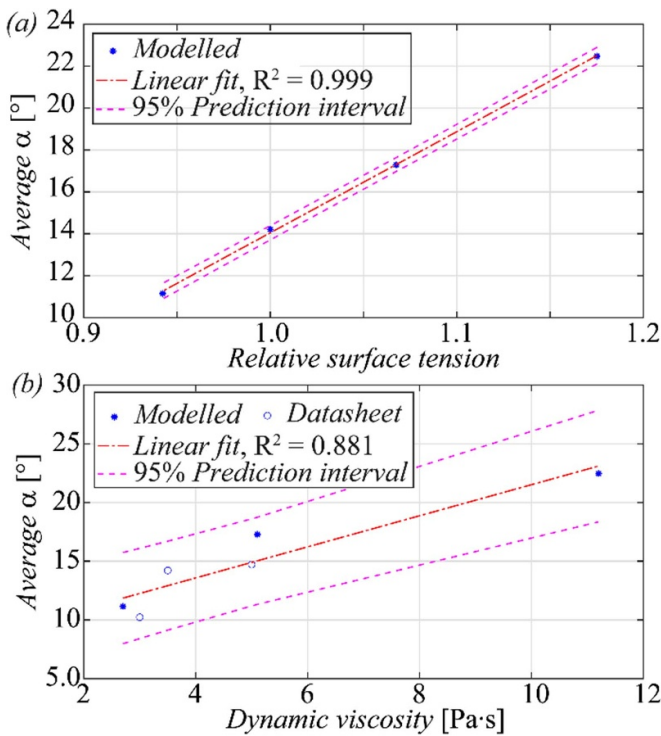


**Figure 8.** Folding angle as a function of relative surface tension (a) and viscosity (b). The angles are the averages taken from figure 5, surface tensions modeled as described in [14] and viscosity as in [13].

its skin-facing frontside. For example, to keep a frontside temperature of 43 °C, the backside would be several degrees hotter, which could be a substantial health risk, since burns form much more quickly at temperatures above 45 °C. The folded

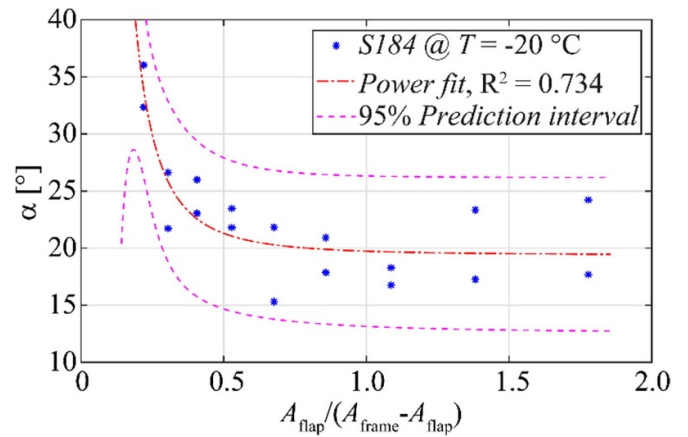


**Figure 9.** Folding angle as a function of the ratio between the flap area and its frame, i.e. surrounding open area.

heater, on the other hand, would have a colder, and hence safer, backside.

The ability of the folded heaters to deliver heat not only more efficiently, but also quickly can have other great advantages. A previous publication [17], have shown that it is possible to monitor arterIALIZED blood gas levels without constantly heating the skin. This is because the vasodilation that instigates the arterIALIZATION of the cutaneous blood flow is not caused by the heat itself, but by a nerve stimulated, local axon reflex triggered by the heat. This study showed that a short heat pulse, up to 15 s long, could trigger an extended vasodilation of up to 180 s, i.e. a duty cycle of about 8%. Hence, it is possible to achieve continuous vasodilation without continuous heating, as long as the heater can deliver a warm enough pulse to trigger the local axon reflex, a conclusion that is

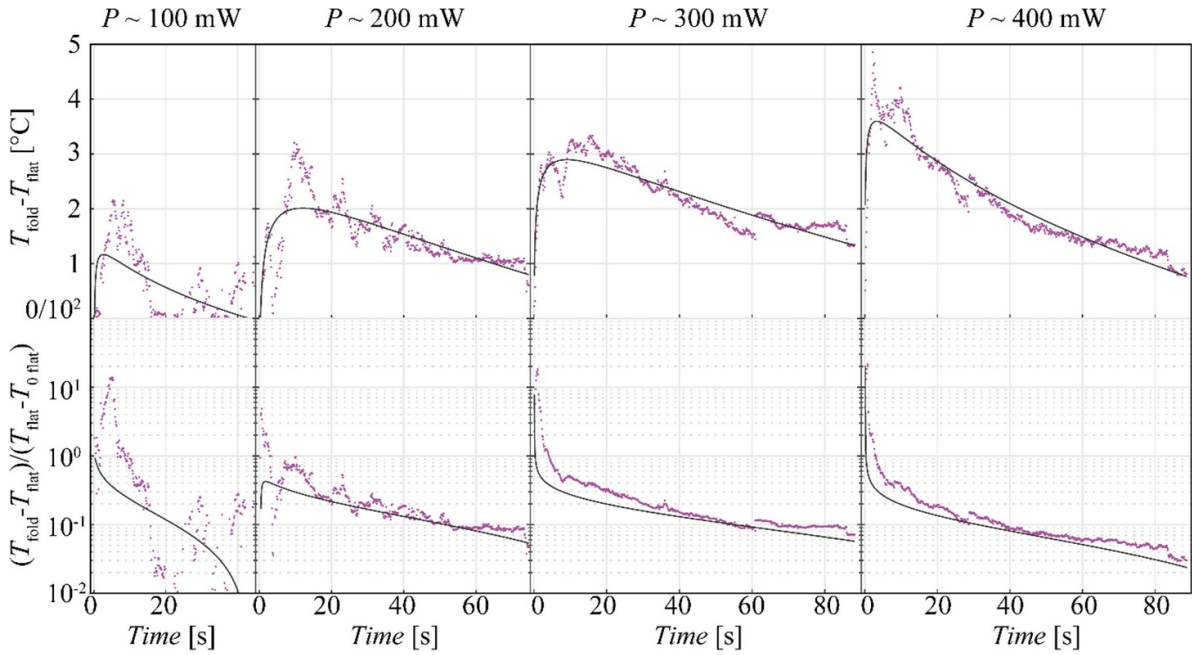


**Figure 10.** Surface temperature difference between the prototype (folded) and reference (flat) heaters over time.

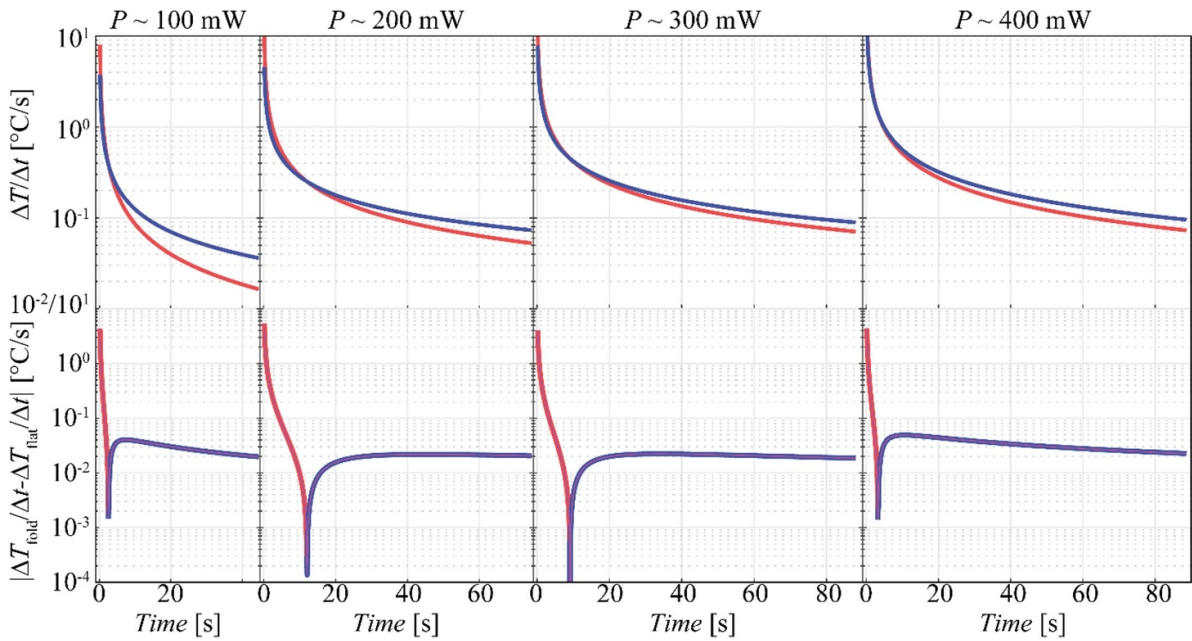


**Figure 11.** Temperature change over time. The top row shows the temperature increase, red lines for the folded prototype heater and blue for the flat reference one. The bottom row shows the absolute value of the difference between the two. The outline colors in the bottom row indicate which of the two heaters have a higher temperature change.

further supported by the findings of, e.g. Magerl *et al* [18] and Nieuwenhoff *et al* [19].

Such pulsed heating will most likely to be much gentler to the skin and hence remove, or at least significantly reduce, the risk of burns [20]. This would be a great improvement to TBM in neonatal care, since it is the risk of burns—or rather the potential harm that can come from them—that is regarded as the major pain-point among current users, and makes continuous monitoring impossible. Here, it should also be noted that

the potential improvement of using a pulsed heating scheme is not exclusive to the TBM method presented here, but could be equally advantageous to conventional solutions.

Hence, it is clear that the investigated fabrication technique could offer substantial improvements to the specific application of TBM. However, this should not narrow its potential impact on other applications. In a broader perspective, the ability to fold resistive heating elements out of plane makes it a viable alternative in general applications where

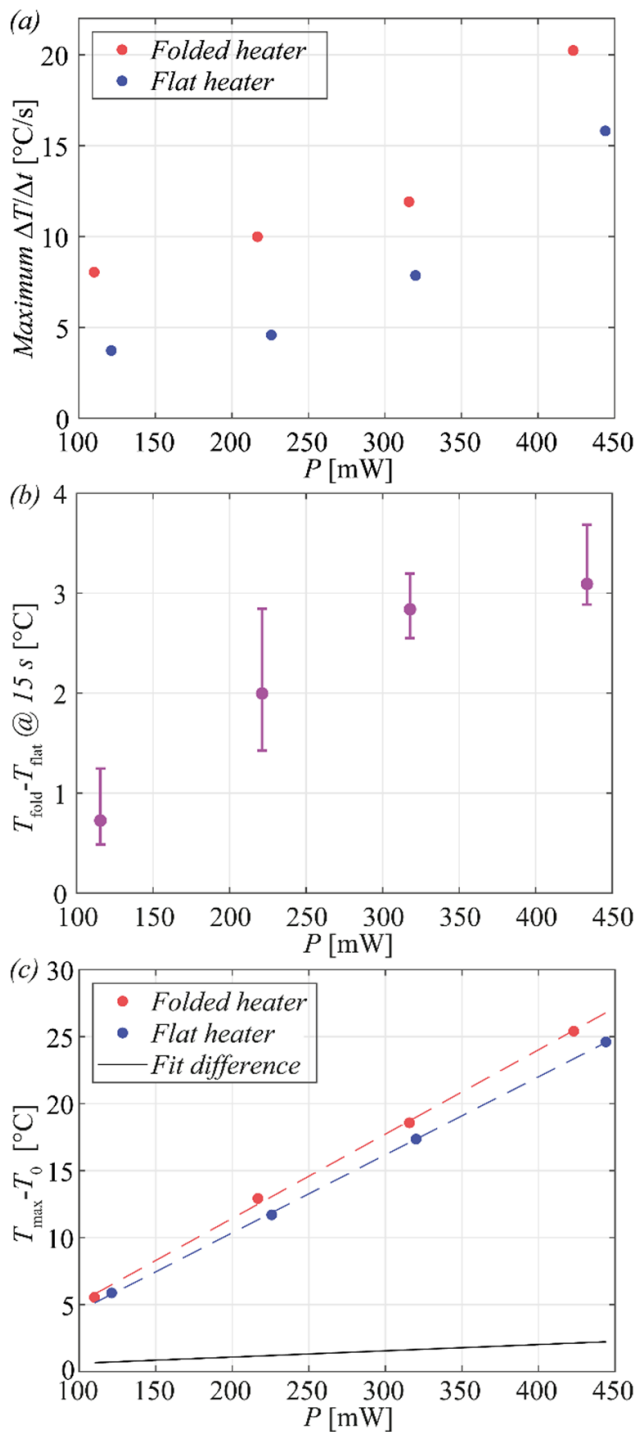


**Figure 12.** (a) Maximum temperature increase rate at the different power levels. (b) Temperature difference between folded and flat heater after 15 s, with bars showing the difference span over the previous second. (c) Semi-steady temperature increase state ( $\Delta T/\Delta t < 0.1 \text{ } ^\circ\text{C s}^{-1}$  and falling),  $T - T_0$ , as a function of applied power for the folded (red) and flat (blue) heaters. The difference between linear fits (dashed lines) to each data set (black) is shown as a reference.

the low thermal conductivity of PDMS has previously been an issue. Moreover, the folding mechanism is by no means limited to simple resistive elements. The presented technique

enables folding of whole PCBs with integrated circuits (ICs) into PDMS. As shown above, stiffer, and hence more, hinges even improved folding, thus leaving ample space for complex, multi-trace circuits integrated on the flaps.

## 5. Conclusion

We have here presented a fabrication process for flexible PCBs with features that fold into PDMS. The process offers both rapid prototyping and as the folding is inherently parallel, it scales up without any inherent per-device time increase. The folding angle of the PCB features could be controlled by the surface tension of the PDMS, and was close to unaffected by all tested design parameters—lengths and widths of both flaps and hinges—and could be selectively eliminated using a hydrophobic surface treatment. However, the study does not present an exhaustive investigation of the parameter space affecting the folding effect. It is likely that flaps, hinges, surface treatments and PDMSs with properties outside the bounds of this study could increase the folding angle beyond the current maximum. Investigating ways of increasing the surface tension of the PDMS by other ways than cooling would be particularly interesting.

Additionally, a set of resistive heaters with their heating elements folded into PDMS were fabricated and evaluated. The evaluation of their heat transfer efficiency, from the PCB to the opposite side of the PDMS, showed a significantly increased surface temperature, as well as an increase in initial thermal response by more than a factor of 10, when compared to an unfolded reference heater. These results alone can make easily fabricated, fast and efficient, resistive heaters a viable option in sensitive temperature control applications where they were previously not. Coupled with the fact that the folding technique offers the possibility of including multiple traces (hinges) onto a folded feature, this opens up the possibility of unprecedentedly complex ICs being incorporated into the bulk of soft PDMS systems without any increase in fabrication time or complexity.

## Data availability statement

The data that support the findings of this study are openly available at the following URL/DOI: [10.5281/zenodo.7414413](https://doi.org/10.5281/zenodo.7414413).

## Acknowledgments

The Knut and Alice Wallenberg foundation is acknowledged for funding the cleanroom facilities. The authors would also like to acknowledge Oskar Hellman and Jan Maslik for their valuable assistance in mask preparation, etching, and PDMS casting.

## ORCID iDs

Ragnar Seton  <https://orcid.org/0000-0002-0379-4526>

Zahra Khaji  <https://orcid.org/0000-0002-5452-7831>  
 Anders Persson  <https://orcid.org/0000-0003-2853-9238>

## References

- [1] Bromley I 2008 Transcutaneous monitoring—understanding the principles *Infant* **4** 95–98
- [2] Ochiai M, Kurata H, Inoue H, Ichiyama M, Fujiyoshi J, Watabe S, Hiroma T, Nakamura T and Ohga S 2020 Transcutaneous blood gas monitoring among neonatal intensive care units in Japan *Pediatr. Int.* **62** 169–74
- [3] Rüdiger M, Töpfer K, Hammer H, Schmalisch G and Wauer R R 2005 A survey of transcutaneous blood gas monitoring among European neonatal intensive care units *BMC Pediatr.* **5** 30
- [4] Kim Y-S, Mahmood M, Kwon S, Maher K, Kang J W and Yeo W-H 2020 Wireless, skin-like membrane electronics with multifunctional ergonomic sensors for enhanced pediatric care *IEEE Trans. Biomed. Eng.* **67** 2159–65
- [5] Seton R, Thornell G and Persson A 2020 Compliance of a microstructured, soft sampling device for transcutaneous blood gas monitoring *RSC Adv.* **10** 36386–95
- [6] Pu Z, Ma J, Li W, Lai X, Su X, Yu H and Li D 2019 A flexible precise volume sensor based on metal-on-polyimide electrodes sandwiched by PDMS channel for microfluidic systems *Microfluid. Nanofluidics* **23** 132
- [7] Guozhen L, Shiqiang L, Liangqi W and Rong Z 2020 Skin-inspired quadruple tactile sensors integrated on a robot hand enable object recognition *Sci. Robot.* **5** eabc8134
- [8] Moon J-H, Baek D H, Choi Y Y, Lee K H, Kim H C and Lee S-H 2010 Wearable polyimide–PDMS electrodes for intrabody communication *J. Micromech. Microeng.* **20** 25032
- [9] Piqué A, Mathews S A, Charipar N A and Birnbaum A J 2012 Laser origami: a new technique for assembling 3D microstructures *Proc. SPIE* **8244** 72–8
- [10] Wang D H and Tan L-S 2019 Origami-inspired fabrication: self-folding or self-unfolding of cross-linked-polyimide objects in extremely hot ambience *ACS Macro Lett.* **8** 546–52
- [11] Zhang Y and Ionov L 2014 Actuating porous polyimide films *ACS Appl. Mater. Interfaces* **6** 10072–7
- [12] Easley J C, Benninger P K R, Shaver H J, Head W S and Piston W D 2009 Rapid and inexpensive fabrication of polymeric microfluidic devices via toner transfer masking *Lab Chip* **9** 1119–27
- [13] Chmielowiec A, Woś W and Gumieniak J 2021 Viscosity approximation of PDMS using Weibull function *Materials* **14** 6060
- [14] Dee T G and Sauer B B 1992 The molecular weight and temperature dependence of polymer surface tension: comparison of experiment with interface gradient theory *J. Colloid Interface Sci.* **152** 85–103
- [15] Seton Ragnar , Khaji Zahra and Persson Anders 2022 PDMS-Polyimide transcutaneous blood gas collector with self-folding out-of-plane heater elements, dataset [Data set] *Zenodo* (<https://doi.org/10.5281/zenodo.7414413>)
- [16] Flowers G L and Switzer S T 1978 *Background Material Properties of Selected Silicone Potting Compounds and Raw Materials for Their Substitutes* (<https://doi.org/10.2172/7032853>)
- [17] Persson A 2021 *System and method for continuous transcutaneous blood gas monitoring*
- [18] Magerl W and Treede R D 1996 Heat-evoked vasodilatation in human hairy skin: axon reflexes due to low-level activity of nociceptive afferents *J. Physiol.* **497** 837–48
- [19] Nieuwenhoff M D, Wu Y, Huygen F J P M, Schouten A C, van der Helm F C T and Niehof S P 2016 Reproducibility of axon reflex-related vasodilation assessed by dynamic thermal imaging in healthy subjects *Microvasc. Res.* **106** 1–7
- [20] Park J-H, Lee J-W, Kim Y-C and Prausnitz M R 2008 The effect of heat on skin permeability *Int. J. Pharm.* **359** 94–103